ORIGINAL ARTICLE

Filters Effect on Image Quality of 177Lu-DOTATATE SPECT Images for Neuro-Endocrine Tumors Scanning

Hussein Dakhil [1], Mohammed Reza Deevband [1*] [ID] , Mahasti Amoui [1], Ahmad Mostaar [1], Mahdi Ghorbani [1], Mohsen Khosroabadi [2], Mohammad Ali Ghodsirad [3]

[1] Department of Bioengineering and Medical Physics, Shahid Beheshti University of Medical Sciences, Tehran, Iran

[2] Department of Medical Physics, North Khorasan University of Medical Sciences, Bojnurd, Iran

[3] Nuclear Medicine Department, Shohada-e-Tajrish Hospital, Shahid Beheshti University of Medical Sciences, Tehran, Iran

*Corresponding Author: Mohammed Reza Deevband
  Email: mdeevband@sbmu.ac.ir

Abstract

Purpose: The quality of the image in SPECT scans depends on the imaging parameters which are determined experimentally in the field of nuclear medicine. Designing a dedicated scanning parameter for ^{177}Lu-DOTATATE SPECT images is required to optimize reconstruction. Therefore, this study aims to evaluate the effect of different filters on image quality for bone SPECT scanning using ^{177}Lu-DOTATATE.

Materials and Methods: The filtered back-projection reconstruction method was used in neuro-endocrine tumor scanning using ^{177}Lu-DOTATATE. Three hours after injection of ^{177}Lu-DOTATATE, SPECT scans from ^{177}Lu-DOTATATE for 30 patients were acquired using a dual-head EvoExel detector system. Seven parameters were considered, including the contrast/noise ratio, injection activity, uptake duration, acquisition time per injection, frame time, measuring time, and type of filters.

Results: In all cases, the application of different filters increased Contrast to Noise Ratio (CNR) (9.1%, 1.8%, 10.9%, 61.8%, 23.6%, 29.1%, and 58.2% for Wiener, Butterworth, Parzen, Metz, Ramp, Shepp-Logan, and Hamming filters, respectively). The percentage of increase in Signal-to-Noise Ratio (SNR) was 3.3%, 1.7%, -24%, 21.7%, 9.8%, 11.9%, and 20.6%.

Conclusion: Based on the quantitative analysis of the results, the application of the Metz filter (power 2) and Hamming filter (with 0.27, 0.47, and 0.67 cut-off frequencies) on SPECT scans of neuro-endocrine tumors is recommended because of their capacity to provide high-quality images.

Keywords: Nuclear Medicine; Image Reconstruction; Filter Design; Image Quality; Single Photon Emission Computed Tomography Imaging.

1. Introduction

Single Photon Emission Computed Tomography (SPECT) is to produce computer-generated images of radiotracer absorption in the immediate environment as a tomographic imaging. It enables the assessment of disease processes using functional and metabolic data from cells and organs [1]. In general, in addition to two-dimensional (2D) images, for lesions that cannot be commented with certainty by imaging the whole body, SPECT images are also taken for diagnosis with higher accuracy and precision from the desired area in the body [1, 2]. Although SPECT images provide three-dimensional information on the distribution of radioactive material, they need to be corrected for radiation attenuation and scattering effects. On the other hand, these images contain few anatomical details, and it is impossible to locate the lesions accurately [3-5].

Previous studies have shown treatment with [177]Lutetium-labeled somatostatin analogs (^{177}Lu-dodecanete traacetic acid tyrosine-3-octreotate (^{177}Lu-DOTATATE)) for patients with neuroendocrine tumors [6]. The SPECT scans are shown by a dual-head, rotating, and variable-angle sodium-iodide scintillation detector. The detectors can be placed in a 90° or a 180° position. Depending on the radiotracer, SPECT acquisition needs a routine scanning time of 20-30 min [7, 8]. Iterative approaches are used to rebuild the SPECT image, which includes photon attenuation correction based on the gamma-ray transmission map and scatter correction [9, 10]. Since the quality of vision in SPECT scans depends on the imaging parameters that are determined experimentally in the field of nuclear medicine, designing a reliable scanning method for ^{177}Lu-DOTATATE/SPECT is needed to diagnose several bone-related conditions [11-15]. In this study, the aim is to evaluate the effect of different filters on image quality for bone scanning using ^{177}Lu-DOTATATE SPECT.

2. Materials and Methods

2.1. Data Collection

SPECT studies were performed using a camera fitted with collimators with Low Energy and High Resolution (LEHR) detectors. Estimates of activity were made at a single time period after ^{177}Lu-DOTATATE injection. All images were reconstructed with a 15-iteration by the FBP algorithm. Attenuation and collimator-detector response compensations were implemented as reported in the literature [1].

2.2. Sample Size Calculation and Patient Selection

Based on the number of patients with inclusion criteria, including demographic characteristics and patient informed consent, sampling was performed by the available sampling method and the number of patients was determined based on previous studies in this field. Considering alpha at 0.1, beta at 0.2, p at 0.05, and d at 0.014 with a confidence level of 95%, using Equation 1, the required sample size was estimated to be 30 patients.

$$n = \frac{(Z_{1-\frac{\alpha}{2}} + Z_{1-\beta})^2 \times p(1-p)}{d^2} = 30 \tag{1}$$

This retrospective study needs the patients' informed consent. Necessary licenses and a code of ethics related to the present research were obtained from the Research Ethics Committee of Shahid Beheshti University of Medical Sciences. SPECT scans of 30 patients were collected from the Shohada-e-Tajrish Hospital. Three hours after injection of ^{177}Lu-DOTATATE, SPECT scans were acquired using a dual-head EvoExel detector system (Siemens Healthiness, Erlangen, Germany). Projections were obtained during 20 minutes at 180 degrees using a parallel hole collimator.

2.3. Image Processing Toolbox

The Image Processing Toolbox (IPT) is a group of functions that increases the capability of the MATLAB numeric calculating environment. This option provides a full-scale set of reference-standard algorithms and programs for image processing, analysis, visualization, and algorithm expansion. It also carries out image segmentation, noise reduction, enhancement, image filtering, filter designing, image restoration, image reconstruction, image registration, geometric transformations, and three-dimensional image processing operations. In this study, MATLAB software (MathWorks Inc., MA) was used to design and apply various image filters. The scanner software had the mentioned filters, but due to the high workload of the software it was preferred to apply the filters in MATLAB software environment.

2.4. Image Acquisition

Patients received 100-200 mCi of ^{177}Lu – DOTATATE, and imaging was performed three hours later. When the frontal or posterior whole-body scanning was performed with twin-head cameras, a 256×1024 matrix with > 1.5 million counts was employed. SPECT volumes are typically selected based on a visual examination of the whole-body planar scan. Since the study focuses on neuro-endocrine tumors, SPECT imaging was performed on all patients with suspicious planar lesions in the region of interest regardless of the patient's diagnosis.

2.5. Filter Design

Different filters used in SPECT imaging may provide optimal results in processed images in different ways, for example, eliminating star artifacts, suppressing noise, or increasing and restoring signal. The filter employed for a certain image processing task is frequently a compromise between the degree of noise reduction, fine detail suppression, and contrast enhancement sought, as well as the spatial frequency pattern of the underlying image data.

2.6. Image Analysis

Filtered Back Projection (FBP) processed into SPECT images using MATLAB software and also Fourier transform of images in MATLAB were performed by own write script code. Images were analyzed in the same workstation.

After applying different filters to the images, Regions of Interest (ROIs) in the tumor and in the background were determined and the mean and standard deviation of these two ROIs were obtained. Then, using Equations 2, 3, and 4, the desired parameters were obtained to evaluate and compare the effect of different filters on the images.

$$SNR = \frac{ROI}{\sigma} \qquad (2)$$

Where SNR refers to signal-to-noise ratio, ROI is the mean region of interest value and σ is the standard deviation of ROI values.

Contrast to Noise Ratio (CNR) was calculated by the following Equation 3:

$$CNR = \frac{|ROI_l - ROI_b|}{\sqrt{\sigma_l^2 + \sigma_b^2}} \qquad (3)$$

Where ROI_l is the mean region of interest value on the tumor, ROI_b is the mean region of interest value on the background which is outside the tumor but inside the same organ, σ_l is the standard deviation of ROI_l values and σ_b is the standard deviation of ROI_b values. Also, contrast was presented by (Equation 4):

$$Contrast = \frac{ROI_l - ROI_b}{ROI_l + ROI_b} \qquad (4)$$

The resolution of the gamma camera is defined in terms of Full Width at Half Maximum (FWHM) measured from a point-source profile. To calculate FWHM, a Gaussian function was fit to the point-source profile and the resolution parameters using the full width at percent maximum relation which is defined in Equation 5.

$$FWHM = 2\sqrt{-2 \times ln\,(2)}\,\sigma \qquad (5)$$

The resolution was calculated and the results were reported using Equation 6.

$$f(x) = Ae^{-(\frac{x-\mu}{\sigma})^2} \qquad (6)$$

Where A is constant according to the normalizing rules, μ is the mean value of x_i, and σ is the standard deviation.

3. Results

3.1. Calculation of Resolution

The resolution of the gamma camera is defined in terms of FWHM measured from a point-source profile. An image of a point source, as shown in Figure 1 (part a), was taken to calculate the resolution and Modulation Transfer Function (MTF) of the imaging system. The profiles obtained from the point source image are shown in Figure 1 (part b). A Gaussian function was fitted to the obtained profiles for the calculation of resolution is shown in Figure 1 (part c).

After designing different filters and applying them to the point source image, the results of the effect of different filters on the resolution were evaluated. These results are listed in Table 1.
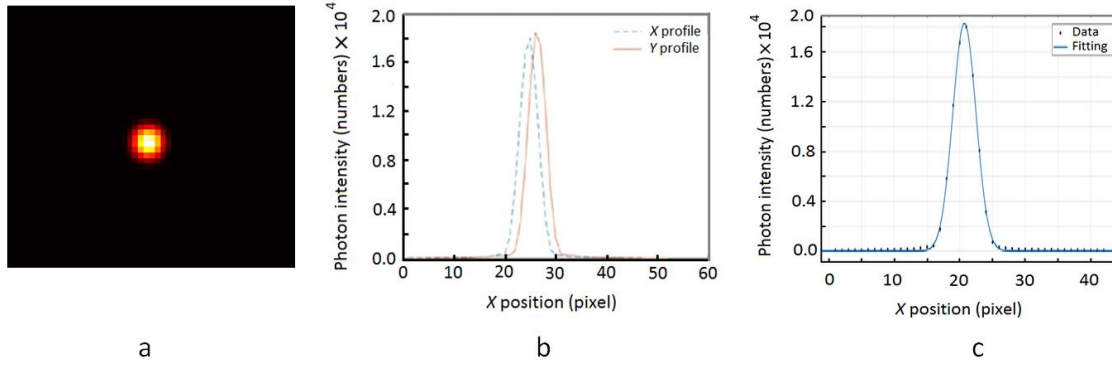
Figure 1. Image of a point source which is taken by gamma camera (a). Profiles obtained by column-wise and row-wise summations of the left image (b). Gaussian function fitted to the profile in the X-direction (c)

Table 1. Parameters of the Gaussian function and the resolution and related fitting accuracy of the Gaussian function

	Parameters	X-Direction	Y-Direction
	A	1.83×10^4	1.89×10^4
	μ	20.71	23.33
	σ	2.50	2.43
	FWHM (mm)	20.50	19.98
Goodness of fit	SSE	8.55×10^5	8.89×10^5
	R-square	0.99	0.99
	Adjusted R-square	0.99	0.99
	Root mean square error (RMSE)	148.11	142.23

3.2. Calculation of Modulation Transfer Function (MTF)

For the purpose of validation of the point source definition, the MTF was calculated. The Fourier transform of the Point Spread Function (PSF) of the point source for calculation of the MTF of the system was obtained, which is shown in Figure 2.

The results for calculating FWHM after applying different filters to the point source profile are listed in Table 2.
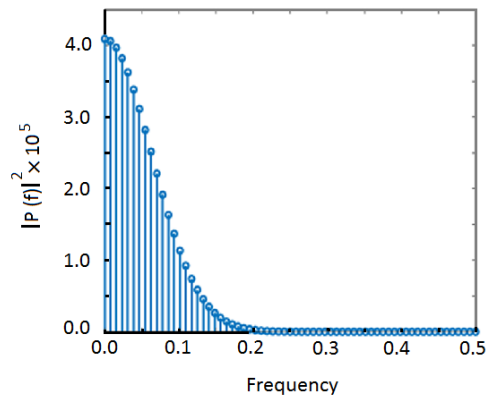

Figure 2. The magnitudes of the fast Fourier transform (MTF) of the point source

Table 2. FWHM values after applying different filters

Filter type	Resolution-X	Resolution-Y
None	20.50	19.98
Wiener	20.62	20.03
Butterworth (power=2)	20.57	20.02
Parzen	16.14	15.86
Metz (power=2)	22.93	22.37
Ramp	21.51	20.98
Shepp-Logan	21.74	21.20
Hamming	22.80	22.24

3.3. Image Quality Analysis

After applying different filters to the images, regions of interest (ROIs) in the lesion and in the background were drawn, and the mean and standard deviation of these two ROIs were obtained (Figure 3). Then, the image quality parameters were obtained to evaluate and compare the effect of various filters on the images. The results of CNR, contrast and SNR are presented in Figures 4, 5 and 6, respectively.
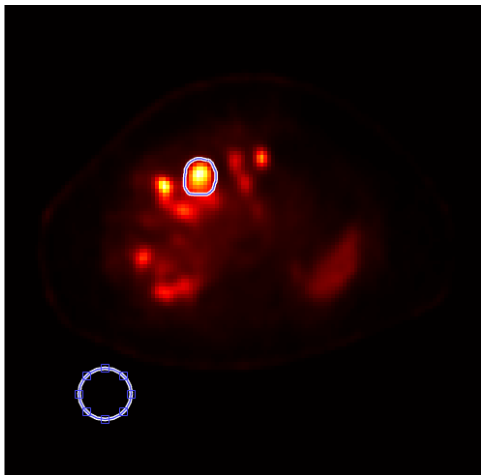

Figure 3. Selected ROIs in the lesion and in the background

As a result, the contrast, CNR, and SNR values for each filter were determined. However, each filter type has a wide range of CNR, contrast, and SNR values owing to the variable combination of filter settings utilized. To determine the filter's overall capability (in terms of CNR, contrast, and SNR production), the mean CNR, mean contrast, and mean SNR were determined. The optimal filter for qualitative and quantitative analysis was selected to have the maximum of mean CNR, contrast, and SNR. The results of the effect of different filters on the image quality parameters are listed in Table 3.
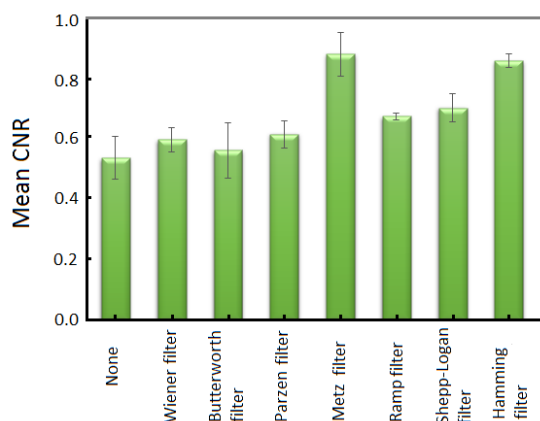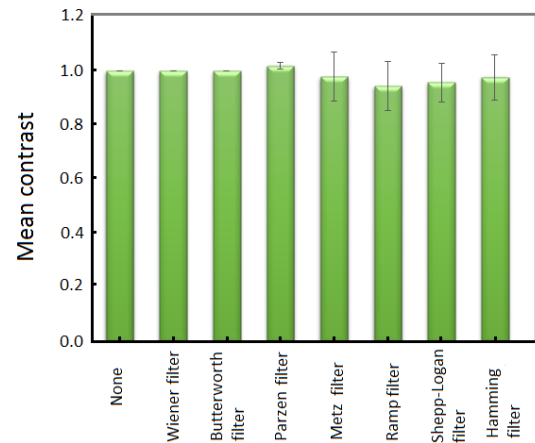

Figure 4. Mean CNR values for different filters

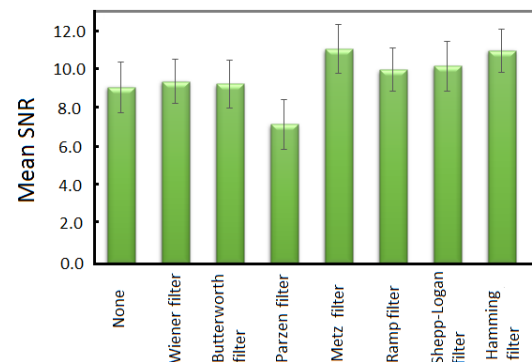**Figure 5.** Mean contrast values for different filters

Figure 6. Mean SNR values for different filters

4. Discussion

Digital filtering of SPECT images is accomplished by choosing a window function from a list of one-dimension filters to employ in reconstruction, examining the generated image slices. Then this process was repeated with a new window function if the results were unsatisfactory. The two-dimension image restoration algorithms discussed in this study adapt spontaneously to the image being processed, obviating the need for repetitive reconstructions. They have been demonstrated to significantly improve image contrast and reduce noise levels compared to Ramp filter reconstructions, all at the expense of a minor increase in execution time when an array processor is utilized. The improvement occurs because the filters modify the frequency and noise components in the image of the object.

As a result, noise develops, which may obstruct the identification of minor lesions. This fact should be considered anytime when digital filtering is employed, and filters should be designed to minimize the risk of

Table 3. Effect of different filters on image quality parameters

Filter type		Mean CNR ± SD	Mean contrast ± SD	Mean SNR ± SD
None		0.55 ± 0.07	1.00 ± 0.00	9.18 ± 1.32
Wiener		0.60 ± 0.03	0.99 ± 0.0001	9.48 ± 1.16
Butterworth (power =2)	Cut-off frequency = 0.27	0.5 ± 0.05	0.98 ± 15.31 E-06	8.63 ± 0.92
	Cut-off frequency = 0.47	0.56 ± 0.09	1.00 ± 7.42E-06	9.34 ± 1.24
	Cut-off frequency = 0.67	0.35 ± 0.13	0.89 ± 23.12 E-06	8.65 ± 1.36
Butterworth (power =4)	Cut-off frequency = 0.27	0.33 ± 0.21	0.85 ± 8.28E-06	5.88 ± 0.98
	Cut-off frequency = 0.47	0.41 ± 0.01	1.00 ± 4.14E-06	6.33 ± 0.84
	Cut-off frequency = 0.67	0.55 ± 0.13	1.32 ± 6.32E-06	6.11 ± 1.32
Butterworth (power =6)	Cut-off frequency = 0.27	0.36 ± 0.08	1.12 ± 5.5E-06	6.12 ± 0.59
	Cut-off frequency = 0.47	0.26 ± 0.05	1.00 ± 2.65E-06	5.14 ± 0.64
	Cut-off frequency = 0.67	0.32 ± 0.08	1.32 ± 6.54E-06	5.83 ± 0.51
Parzen	Cut-off frequency = 0.27	0.60 ± 0.11	0.99 ± 0.03	6.98 ± 0.12
	Cut-off frequency = 0.47	0.62 ± 0.05	1.02 ± 0.01	7.2 ± 1.28
	Cut-off frequency = 0.67	0.61 ± 0.12	1.08 ± 0.13	8.12 ± 2.11
Metz (power=2)		0.89 ± 0.07	0.97 ± 0.09	11.17 ± 1.25
Metz (power=4)		0.74 ± 0.18	0.81 ± 0.87	9.54 ± 0.85
Ramp	Cut-off frequency = 0.27	0.48 ± 0.02	0.91 ± 0.07	9.11 ± 0.97
	Cut-off frequency = 0.47	0.68 ± 0.01	0.94 ± 0.09	10.08 ± 1.13
	Cut-off frequency = 0.67	0.61 ± 0.03	0.98 ± 0.11	9.98 ± 1.01
Shepp-Logan	Cut-off frequency = 0.27	0.81 ± 0.13	0.85 ± 0.61	9.81 ± 3.13
	Cut-off frequency = 0.47	0.71 ± 0.04	0.96 ± 0.07	10.27 ± 1.29
	Cut-off frequency = 0.67	0.75 ± 0.01	0.85 ± 0.12	9.85 ± 1.23
Hamming	Cut-off frequency = 0.27	0.71 ± 0.02	0.92 ± 0.04	10.45 ± 0.92
	Cut-off frequency = 0.47	0.87 ± 0.02	0.97 ± 0.08	11.07 ± 1.14
	Cut-off frequency = 0.67	0.88 ± 0.03	0.95 ± 0.06	10.95 ± 1.05

this danger. The choice between pre-reconstruction and post-reconstruction filtering of SPECT studies is not entirely clear, as it is illustrated in Table 3. Pre-reconstruction filtering is favorable for the following reasons. First, the noise power spectrum of the planar image is more accessible to estimate the SPECT images. Second, with 2D pre-reconstruction filtering, the value delivered to the back-projector is calculated at each position, there for a more significant statistical sampling is employed (i.e., the whole data set is filtered, not only one slice). This is critical since SPECT imaging is photon-limited, and the extra information in adjacent slice scans aids in noise reduction and contrast enhancement. Third, the blurring of nuclear medicine images is 2D. Hence, techniques for 2D resolution recovery should be used to preprocess the data. This, together with the higher statistical sample size, enables the back-projector to receive more accurate input data, resulting in enhanced SPECT images. Finally, for reconstructing slices with an oblique angle from transverse slices, pre-reconstruction filtering with a 2D symmetric filter produces an image with an isotropic point response [16]. It was verified that for a given spatial location, the FWHM varies only about 1 mm in any direction for the images reconstructed by these filters. There are additionally other advantages, for post-reconstruction filtering. One benefit of post-reconstruction processing for resolution recovery is

that spatial resolution (and MTF) fluctuates less across a given tomographic slice than in planar images as a function of distance from the collimator face. This justifies the usage of a single MTF with deconvolution.

Additionally, only the slices that have been reassembled must be processed. This is of little consequence when an array processor is utilized to decrease execution time, but when a minicomputer is used alone, the time savings are possibly considerable. It is tough to choose between Wiener and count-dependent Metz filtering. The Wiener filter has an excellent theoretical base and adjusts the image's noise level, object power spectrum, and image blurring (system MTF). Although the count-dependent Metz filter, as constructed, responds exclusively to changes in noise level, it does have a speed advantage over the Wiener filter due to its simplicity. No discernible difference was seen in image quality with clinical images when any of these approaches were used to filter the SPECT scans. This is possibly a result of the minor variance in object power spectra for many clinical nuclear medicine images compared to the variation produced by various total counts, or it is possibly because both filters are optimized by minimizing the MSE.

Based on the data in Table 3, the Metz filter (power 2) and the Hamming filter (with 0.27, 0.47, and 0.67 cut-off frequencies) have higher values for CNR, contrast, and SNR. Therefore, based on the quantitative analysis of the results, the application of the Metz filter (power 2) and the Hamming filter (with 0.27, 0.47, and 0.67 cut-off frequencies) on SPECT scans of neuro-endocrine tumors is recommended due to their capacity to provide high-quality images.

Actually, there are various image reconstruction algorithms in nuclear medicine (such as Ordered Subset Expectation Maximization (OSEM) [14, 15, 17] and Maximum-Likelihood Expectation-Maximization (MLEM) [18-19]). On the other hand, the FBP algorithm is more often used in whole-body scanning in Shohada-e-Tajrish Hospital and this was used in this study. This is a limitation of the present study and a comparison between the results from the FBP algorithm and OSEM and MLEM algorithms can be a subject for future research.

5. Conclusion

Based on the quantitative analysis of the results, the application of Metz filter (power 2) and the Hamming filter (with 0.27, 0.47, and 0.67 cut-off frequencies) on SPECT scans of neuro-endocrine tumors is recommended because of their capacity to provide high-quality images.

Acknowledgements

References

1- Elettra Merola, Maria Rinzivillo, Noemi Cicchese, Gabriele Capurso, Francesco Panzuto, and Gianfranco Delle Fave, "Digestive neuroendocrine neoplasms: A 2016 overview." *Digestive and Liver Disease,* Vol. 48 (No. 8), pp. 829-35, (2016).

2- Nitya Raj, Nicola Fazio, and Jonathan Strosberg, "Biology and systemic treatment of advanced gastroenteropancreatic neuroendocrine tumors." *American Society of Clinical Oncology Educational Book,* Vol. 38pp. 292-99, (2018).

3- Kjell Öberg and Daniel Castellano, "Current knowledge on diagnosis and staging of neuroendocrine tumors." *Cancer and metastasis reviews,* Vol. 30 (No. 1), pp. 3-7, (2011).

4- Tim Van den Wyngaert *et al.*, "The EANM practice guidelines for bone scintigraphy." *European journal of nuclear medicine and molecular imaging,* Vol. 43 (No. 9), pp. 1723-38, (2016).

5- Cheng-Kai Huang, Jay Wu, Kai-Yuan Cheng, and Lung-Kwang Pan, "Optimization of imaging parameters for SPECT scans of [99mTc] TRODAT-1 using Taguchi analysis." *PLoS One,* Vol. 10 (No. 3), p. e0113817, (2015).

6- Samer Ezziddin *et al.*, "Predictors of long-term outcome in patients with well-differentiated gastroenteropancreatic neuroendocrine tumors after peptide receptor radionuclide therapy with 177Lu-octreotate." *Journal of nuclear medicine,* Vol. 55 (No. 2), pp. 183-90, (2014).

7- Simron Singh *et al.*, "Consensus recommendations for the diagnosis and management of pancreatic neuroendocrine tumors: guidelines from a Canadian National Expert Group." *Annals of Surgical Oncology,* Vol. 22 (No. 8), pp. 2685-99, (2015).

8- Ali Afshar-Oromieh *et al.*, "The theranostic PSMA ligand PSMA-617 in the diagnosis of prostate cancer by

PET/CT: biodistribution in humans, radiation dosimetry, and first evaluation of tumor lesions." *Journal of nuclear medicine,* Vol. 56 (No. 11), pp. 1697-705, (2015).

9- Clemens Kratochwil *et al.*, "[177Lu] lutetium-labelled PSMA ligand-induced remission in a patient with metastatic prostate cancer." *European journal of nuclear medicine and molecular imaging,* Vol. 42 (No. 6), pp. 987-88, (2015).

10- Ambikalmajan MR Pillai and Furn F Russ Knapp, "Editorial (Thematic Issue: Lutetium-177 Labeled Therapeutics: 177Lu-PSMA is Set to Redefine Prostate Cancer Treatment)." *Current Radiopharmaceuticals,* Vol. 9 (No. 1), pp. 6-7, (2016).

11- Ahmet Peker, Okan Çiçek, Çiğdem Soydal, Nuriye Özlem Küçük, and Sadık Bilgiç, "Radioembolization with yttrium-90 resin microspheres for neuroendocrine tumor liver metastases." *Diagnostic and Interventional Radiology,* Vol. 21 (No. 1), p. 54, (2015).

12- Emilio Mezzenga *et al.*, "Quantitative accuracy of 177Lu SPECT imaging for molecular radiotherapy." *PLoS One,* Vol. 12 (No. 8), p. e0182888, (2017).

13- Tobias Rydén, Martijn Van Essen, Ida Marin, Johanna Svensson, and Peter Bernhardt, "Deep-learning generation of synthetic intermediate projections improves 177Lu SPECT images reconstructed with sparsely acquired projections." *Journal of nuclear medicine,* Vol. 62 (No. 4), pp. 528-35, (2021).

14- Eero Hippeläinen, Mikko Tenhunen, Hanna Mäenpää, and Antti Sohlberg, "Quantitative accuracy of 177 Lu SPECT reconstruction using different compensation methods: phantom and patient studies." *EJNMMI research,* Vol. 6 (No. 1), pp. 1-8, (2016).

15- E Grassi *et al.*, "Impact of a commercial 3D OSEM reconstruction algorithm on the 177Lu activity quantification of SPECT/CT imaging in a Molecular Radiotherapy trial." *Radiol Diagn Imaging,* Vol. 1 (No. 1), pp. 1-7, (2017).

16- Jeffrey A Norton, "Surgery for primary pancreatic neuroendocrine tumors." *Journal of gastrointestinal surgery,* Vol. 10 (No. 3), pp. 327-31, (2006).

17- Tiwari S, Srivastava R. "An OSEM-based hybrid-cascaded framework for PET/SPECT image reconstruction." *Int J Biomed Engin Technol*; 18(4): 310-332, (2015).

18- Kim G, Lim I, Song K, Kim JG. "Super-spatial resolution method combined with the maximum-likelihood expectation maximization (MLEM) algorithm for alpha imaging detector." *Nucl Engin Technol*; 54(6): 2204-2212, (2022).

19- Wang H, Yang Y, Dou G, Lou J, Zhu X, Song L, et al. "A 3D reconstruction method of bubble flow field based on multi-view images by bi-direction filtering maximum likelihood expectation maximization algorithm." *Int J Multiphase Flow*; 165: 104480, (2023).